PETROPHYSICS

The Group's approach is essentially that of materials science. We observe and seek to understand the physical behaviour of geological materials under controlled laboratory conditions, and then apply such insights to the structure and processes of the Earth. Measurements of macroscopic physical properties (e.g., strength, or seismic wave speeds and attenuation) are interpreted through microstructural studies centred around light and electron microscopy. Often it is necessary to prepare, from either natural or synthetic precursors, simpler synthetic materials whose properties are amenable to more detailed interpretation than those of complex natural rocks. Our interest in geological materials is shared by members of the Petrochemistry and Experimental Petrology Group, who focus primarily upon the chemical aspects of their behaviour.

Geological and geophysical observations of the response of the Earth to naturally applied stresses, which vary widely in magnitude and timescale, provide much of the motivation for the Group's work. In the laboratory, ultrasonic wave propagation and lower frequency forced-oscillation methods are used to probe the elastic/anelastic behaviour which determines seismic wave speeds and attenuation. On longer time scales and at higher stresses, the mechanical behaviour of synthetic faults and fault gouge is studied with particular interest in the complex interaction between chemical reaction, deformation and fluid flow. The fact that all but the simplest elastic behaviour of geological materials is controlled by microscopic defects such as dislocations and processes operative at grain boundaries, places a premium on the complementary microstructural studies involving light and electron microscopy.

Major achievements for 2000 include:

- the first in-situ measurement, at high pressure and temperature, of permeability evolution during concurrent metamorphic reaction and deformation;

- enhancement of our capability for accurate high-temperature measurement of elastic wave speeds by ultrasonic interferometry;

- determination of the grainsize sensitivity of seismic wave attenuation in fine-grained polycrystalline olivine; and

- numerical modelling of co-seismic stress changes around large-displacement faults to examine fluid flow localisation in low-displacement aftershock-generated faults which host gold deposits.

Members of the group collaborate widely within the School and beyond. Natural links with the Seismology Group are based on a common interest in the interpretation of seismological models for the Earth's interior. Preparation of synthetic rock specimens and their precursors and investigations of melt distribution within partially molten upper mantle rocks involve intensive collaboration between the Petrophysics and Petrochemistry and Experimental Petrology Groups. Field-based and modelling studies of coupling between deformation, flow and reaction, especially in hydrothermal ore systems by members of the Centre for Advanced Studies of Ore Systems (RSES and Geology Department, Faculty of Science), complement the experimental program in rock deformation.

Within the wider ANU community, the influence of the Petrophysics Group is felt in a variety of forums. The flagship analytical TEM to serve the needs of the ANU materials science community, housed within the School, is being operated by Dr J. Fitz Gerald and Mr D. Llewellyn on behalf of the ANU Electron Microscope Unit. In this capacity, Dr J. Fitz Gerald collaborates intensively in microstructural aspects of various materials science programs of the Research School of Physical Sciences and Engineering. In 2000, the Group maintained its strong commitment to the enrichment of undergraduate/graduate teaching. Dr I. Jackson presented eighteen lectures and associated tutorials on Seismology and Physics of Earth Materials, amounting to half of the undergraduate physics unit PHYS2018.

The departures during the year of Drs Sharon Webb and Shuqing Zhang have inevitably cost the Group considerable momentum in its major research activities during the latter part of the year. Fortunately this has been offset to some degree by the benefits of the restructuring of research support undertaken during 1999. The successful operation of novel equipment, and the further development and timely exploitation of associated experimental techniques, depend heavily upon the skill and commitment of Messrs H. Kokkonen and J. Carr and Ms L. Weston along with the staff of the School's Mechanical and Electronics Workshops. Mrs K. Provins provides invaluable administrative support for the activities of the Petrophysics and Ore Genesis Groups, including responsibility for website development and maintenance. We take this opportunity of thanking Drs Webb and Zhang for their major contributions and wishing them well with the next phase of their respective careers.

HIGH-TEMPERATURE SEISMIC PROPERTIES OF EARTH MATERIALS

Inadequate knowledge of the temperature dependence of elastic wavespeeds for key high-pressure minerals continues to be a major barrier to the robust interpretation of seismological models for the Earth's interior in terms of chemical composition, mineralogy and temperature. Coherent polycrystalline specimens of the major transition-zone and lower-mantle phases have been successfully prepared during the past decade, and accurate measurements of the pressure dependence of their elastic wave speeds have been performed. Despite considerable progress in recent years with diamond-anvil based opto-acoustic techniques and with ultrasonic interferometry in multi-anvil apparatus, much less is known about the temperature dependence of elastic wavespeeds.

In addition, there are substantial uncertainties associated with extrapolation of experimental data generally obtained at high frequencies (MHz-GHz) into the realm of low-frequency seismic wave propagation (mHz–Hz). Uncertainties in extrapolation are likely to be particularly important at high temperatures owing to the thermally activated mobility of vacancies and dislocations and their interactions with grain boundaries.

In order to address these issues, we are extending to very high temperature (1300°C) our capability for elastic wavespeed measurement through high-frequency (10-100 MHz) ultrasonic interferometry. In parallel with such studies, direct access to the seismic-frequency regime is provided by equipment, designed and built in house, that measures shear modulus G and the associated strain-energy dissipation Q^{-1} through torsional forced oscillation and microcreep tests.

High-temperature ultrasonic interferometry

S.L. Webb, I. Jackson, D.A. Boness[1] and L.J. Weston

Last year we reported promising measurements of compressional and shear wavespeeds to 1300˚C at 300 MPa pressure on polycrystalline alumina. In that study, acoustic communication between the transducer, acting as both source and receiver of the elastic waves, and the specimen exposed to the high-P–T environment was effected by a compound steel/ alumina/ molybdenum buffer rod. In order to minimise mismatches in thermal expansion presumably responsible for the observed thermal cracking we have this year simplified the buffer-rod geometry by elimination of the Mo component of the buffer rod. Fe foil of 3 μm thickness inserted between the specimen and alumina buffer rod helps provide the necessary intimate mechanical coupling. The new geometry was first tested on synthetic polycrystalline $CaTiO_3$ and Fo_{90} olivine specimens surrounded by CaF_2 serving as a mechanically weak pressure-transmitting medium. In both cases, however, the experiments were compromised by chemical reactions occuring at the highest temperatures between the CaF_2 and the other components of the experimental assembly. For example, for $CaTiO_3$, the result was a $CaTiO_3$-CaF_2-Al_2O_3-Fe melt that penetrated the

[1] Seattle University

$CaTiO_3$ polycrystal as a network of veins resulting in reduced wavespeeds. Exploratory tests indicated that MgF_2, an alternative pressure-transmitting medium, reacts with Fo_{90} olivine at high temperature to produce the humite mineral norbergite.

Failure to identify a suitable halide pressure-transmitting material for very high temperature conditions resulted in a decision to trial soft iron in that role. Preliminary experiments indicate that the compressional wavespeed measured on a fine-grained (3 μm) Fo_{90} olivine polycrystal closely approaches that expected for a dense polycrystal from single-crystal elasticity data, at least for temperatures > 500°C (Figure 1). The much greater scatter evident at lower temperatures may reflect complications associated with the substantial strength of the Fe pressure-transmitting medium.

During the coming year, completion of the measurements on olivine will allow an interesting comparison with low-frequency forced oscillation data (following section). In addition tests on olivine specimens of smaller diameter (down to 3 mm) will be undertaken in order to establish the robustness of the approach for measurement of the necessarily small specimens of high-pressure minerals.

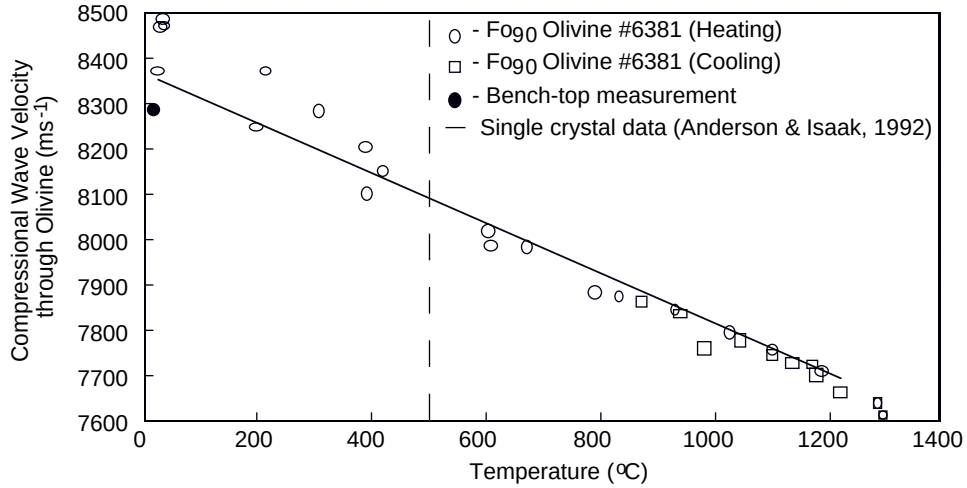

Figure 1: Compressional wavespeed for polycrystalline Fo_{90} olivine determined by ultrasonic interferometry compared with the corresponding temperature-dependent wavespeed (solid line) calculated from published single-crystal elasticity data.

Seismic wave attenuation in polycrystalline olivine: frequency, temperature and grainsize sensitivity

I. Jackson, J.D. Fitz Gerald, U. Faul, H. Kokkonen, J. Carr and B.Tan

Much of the variation of seismic wavespeeds and attenuation in the Earth's upper mantle is attributable to high-temperature viscoelastic relaxation in rocks composed mainly of the mineral olivine. Quantitative interpretation requires rheological data obtained under controlled laboratory conditions on well-characterised materials. In order to build a mechanistic understanding of high-temperature viscoelastic relaxation in such ultramafic materials, we have continued a programme involving fabrication and characterisation of a suite of synthetic polycrystalline olivine aggregates and measurement of their mechanical properties at high temperature through a combination of torsional forced oscillation and microcreep tests.

Specimens of composition Fo_{90} ($[Mg_{0.9}Fe_{0.1}]_2SiO_4$) have been fabricated from pellets of precursor powders by hot-isostatic pressing in an internally heated gas-medium apparatus typically for 25 hr at temperatures of 1200-1300°C and pressures of 200-300 MPa. Additional specimens have been fabricated during the year in $Ni_{70}Fe_{30}$ containers, conducive to the

thermodynamic stability of natural Ni-bearing olivines, from both synthetic (sol-gel) and natural (San Carlos) precursors. Firing of the precursor powders and in some cases also the hot-pressed specimens has allowed the virtual elimination of hydroxyl (<10 ppm) from some specimens.

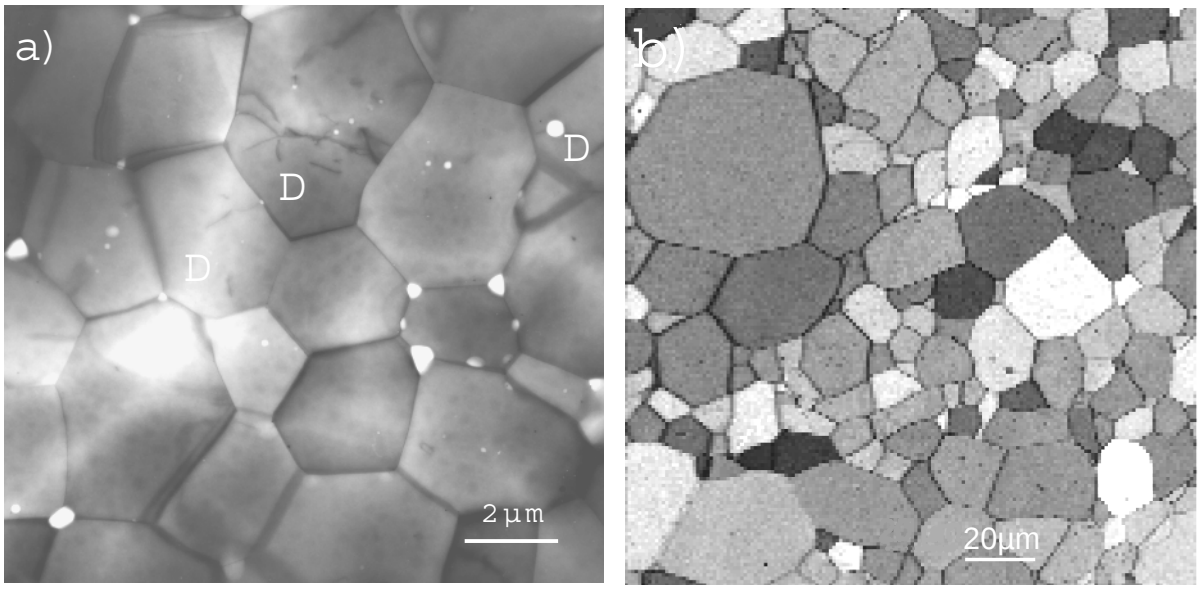

Figure 2: Representative microstructures. (a) TEM bright field image of the most fine-grained specimen of this study. Such sol-gel derived samples have a uniform grain size distribution with near-ideal 'foam textures' and gently curved grain boundaries. Pores are white in this image. The dark lines above the letter D are (rare) dislocations. (b) Band contrast image from an electron-backscatter diffraction (EBSD) map of the most coarse-grained specimen. The grain size distributions of such samples derived from San Carlos olivine are broader than those for the sol-gel derived specimens, but the grain shapes are similarly equate with smoothly curved grain boundaries.

A highlight of this year's activity has been the completion of a study of the viscoelastic behaviour of four texturally well-equilibrated, essentially melt-free specimens ranging in mean grainsize from 3 to 23 µm (Figure 2). They are generally of low dislocation density and contain low concentrations of impurity. In the materials of natural origin, trace amounts of CaO and Al_2O_3 are detected in the grain boundaries, and small amounts of glass (<< 0.1 vol %) representing melt formed at high temperature, are present mainly in grain-edge tubules. In the materials of sol-gel origin, local departures from ideal olivine stoichiometry are manifest in widely distributed orthopyroxene (± magnesiowüstite) grains, but no melt has been detected.

Measurement in the forced oscillation tests of the amplitudes and relative phase of the applied alternating torque and the resulting angular distortion of the cylindrical specimen yield determinations of the shear modulus G and associated dissipation Q^{-1}, typically for oscillation periods of 1–100 s. Complementary information concerning the material response at longer periods and a measure of the recoverability of the non-elastic deformation are obtained from torsional microcreep tests to maximum shear strains of order 10^{-5}.

With increasing temperature T above 900°C, these materials become markedly viscoelastic, displaying both intense dissipation and associated frequency dependence (dispersion) of the shear modulus (Figure 3). A mixture of anelastic (recoverable strains) and viscous (irrecoverable) processes is involved — the latter assuming a progressively more important role

with increasing temperature and timescale. Various considerations including grainsize sensitivity

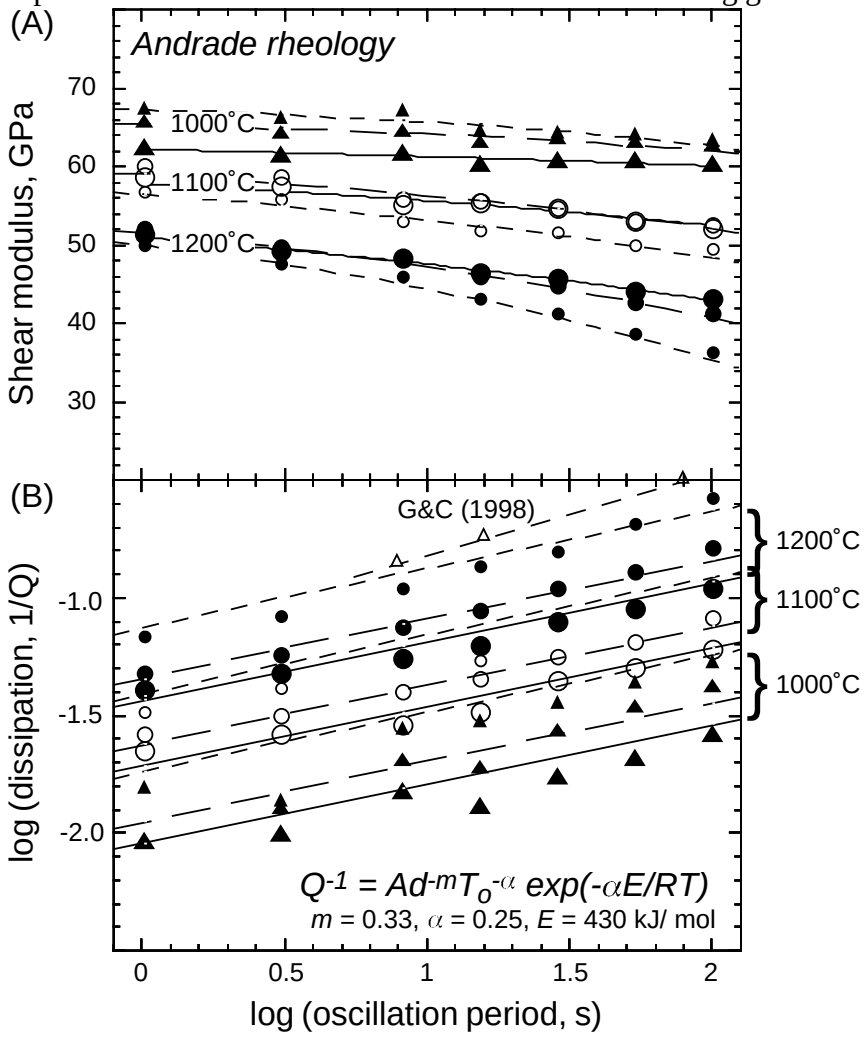

Figure 3: Comparison of the high-temperature mechanical behaviour of specimens with average grainsizes of 23, 12 and 3 μm. The diameters of the plotting symbols are scaled to reflect average grainsize and likewise the continuous, long-dashed and short-dashed curves are associated with the coarse-, medium- and fine-grained specimens, respectively. (a) Shear modulus. Curves labelled with temperature indicate the modulus dispersion associated with Andrade models fitted simultaneously to $G(T_0)$ and $Q^{-1}(T_0)$. (b) log (dissipation). Lines represent the fit of the displayed equation to the entire 1000-1300˚C, 1-100 s dataset for all four specimens, except for the uppermost line representing the results of Gribb and Cooper (1998) *J. Geophys. Res. 103, 27267-27279,* for a resynthesized dunite of 2.8 μm grainsize at 1200˚C.

and the magnitude of the activation energy combine to implicate diffusional processes operative mainly in grain-boundary regions as the cause of the viscoelastic behaviour. Extrapolation of the relatively mild grainsize sensitivity ($Q^{-1} \sim d^{-1/3}$) to the 1–10 mm grainsizes representative of the Earth's upper mantle suggests that much of the dissipation observed seismologically might be attributable to these grain-boundary processes (Figure 4).

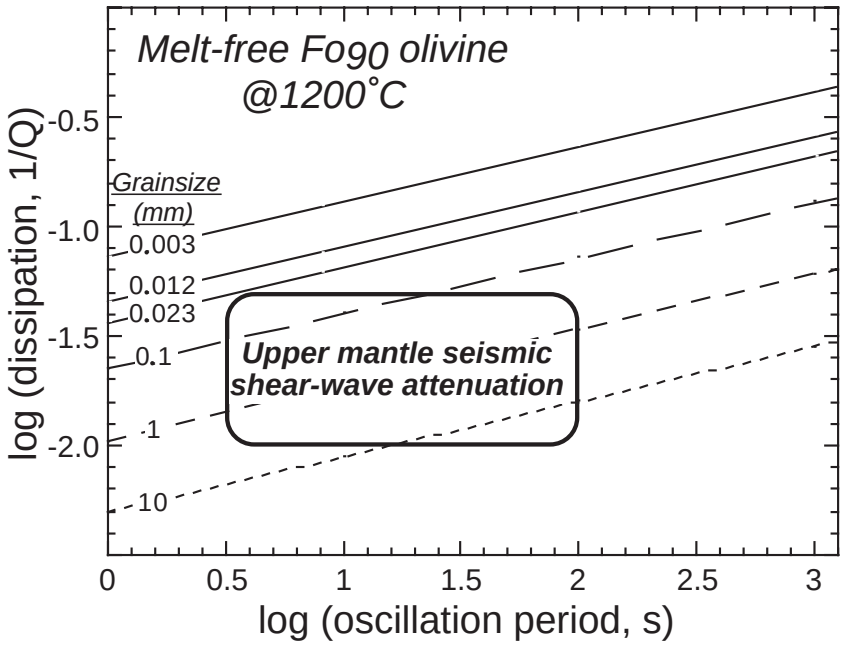

Figure 4: Extrapolation of the grainsize sensitivity of Q^{-1} measured at 1200˚C to grainsizes considered representative of the upper mantle. Solid curves represent the fit to experimental data, broken curves the extrapolation to mantle grainsize. The box represents observations of seismic shear wave attenuation in the upper mantle.

FLUID FLOW DURING CRUSTAL DEFORMATION, METAMORPHISM AND ORE GENESIS

Fluid flow and fluid-rock reaction processes at depth in the Earth's crust influence many important aspects of crustal dynamics, including mass transport, the evolution of crustal strength, earthquakes, and the formation of many types of ore deposits. Deformation processes, which act to modify the permeability of rocks, are complexly coupled with flow and reaction processes.

Members of the Petrophysics Group apply fundamental, high-pressure, high-temperature experimental approaches to investigate coupling between deformation, reaction and fluid transport properties in rock materials. Our rock deformation laboratory has facilities which allow in situ measurement of permeability in small rock samples at temperatures up to 1000°C confining pressures up to 300 MPa, and pore fluid pressures up to 300 MPa. We are currently using this equipment to explore how competition between deformation and fluid-infiltration-driven reactions influences permeability evolution in metamorphic systems.

The experimental program is complemented by field-based, microstructural and numerical modelling studies of linkages between localisation of deformation and development of ore-hosting hydrothermal systems. This work (reported in the Ore System Studies part of this Annual Report) focusses mainly on how, during the evolution of shear systems, fluid flow, reaction and ore deposition can become localised within a small subset of the total population of co-active faults and shear zones. The synergy between complementary field-based, experimental and numerical studies in the Petrophysics Group provides a powerful approach to problems in crustal fluid flow.

Fluid flow and deformation during model contact metamorphism

S. Zhang, J.D. Fitz Gerald and S.F. Cox

In 1999, we reported an exploratory experimental study on the evolution of permeability and porosity during the water-infiltration-driven decarbonation reaction of Calcite + Quartz = Wollastonite + CO_2. This set of experiments was conducted under isostatic conditions and the permeability was controlled by two competing processes: porosity reduction due to local deviatoric-stress-driven plastic deformation, and porosity increase due to solid volume decrease associated with the decarbonation. Early this year, we incorporated concurrent axial deformation in the specimen undergoing this decarbonation reaction. The purpose of this set of experiments was to test an intuitive concept that the strength for materials undergoing mineral reactions is controlled by the competition between reaction-induced volumetric strain rate and the imposed deformation rate. For the reaction of Calcite + Quartz = Wollastonite + CO_2, the solid volume reduction is about 34%. At 700°C, the reaction goes to completion within about 10 hours for a mixture containing about 10 wt% quartz. Thus the volumetric strain rate is about 2×10^{-6} s^{-1}. If imposed compressive strain rate is lower than about 7×10^{-7} s^{-1}, the material during reaction will have nominally 'zero' strength. In the new set of deformation experiments, we applied an axial deformation rate about one order of magnitude faster than the reaction-induced volumetric strain rate. We examined how concurrent deformation and mineral composition influenced reaction progress and how reaction progress in turn affected the deformation behavior.

We used synthetic calcite/quartz mixtures containing 5 to 50 wt% of quartz particles. The initial particle sizes of calcite and quartz are 2-3 μm and 30-50 μm, respectively. For comparison, experiments were also conducted on pure calcite, pure quartz, and pure wollastonite. Pure wollastonite was produced by decarbonation reaction between equimolar calcite and quartz. The experimental conditions are: confining pressure 225 MPa, water pore pressure 200 MPa, temperature 700°C, axial strain up to 20%, and axial strain rate about 5×10^{-6} s^{-1}.

The deformation of calcite/quartz mixtures undergoing decarbonation reaction is characterized by a sharp strength increase with increasing strain (strain hardening), which is largely a result of formation of high strength wollastonite aggregates. Samples initially containing higher amounts of quartz have higher strength. The concurrent deformation did not appear to significantly modify either the fluid permeability or the reaction progress. The reaction rate decreased markedly with increasing volume of quartz particles, suggesting the importance of calcite reaction surface area within the specimen in controlling reaction progress. The experiments provide a complete set of data for studying deformation mechanisms and mechanical strength within multi-component systems. Detailed analysis of the experimental results is underway.

MICROSTRUCTURAL STUDIES

Slip and recrystallization in plagioclase - new experiments

H. Stünitz[2], J.D. Fitz Gerald and J. Tullis[3]

Several deformation experiments have been carried out at Brown University using single crystals of plagioclase (An_{60}, volcanic megacryst origin) subjected to conditions that represent as closely as possible those in the Earth's deep crust – 900°C, confining pressure 1 GPa, strainrate 10^{-6} sec^{-1}. The main objective is to explore the microstructural development using light and transmission electron microscopy, with particular emphasis on dislocation generation, slip system details and recrystallization.

---

[2] Geologisch-Paläontologisches Inst., University of Basel, Switzerland

[3] Dept. Geological Sciences, Brown University, Providence RI, USA

Twin structures, dislocations, slip traces, fractures and precipitates are characteristic of the deformed crystals. Careful correlation between microstructures from the specimen scale to the sub-micron scale revealed low-strain zones where dislocations are confined to the vicinity of cracks or healed cracks. Most of these cracks were probably introduced by coring of the plagioclase crystals that was necessary to produce the specimens deformed at Brown University. More uniformly deformed zones are also present, without such obvious dislocation sources, but with significant densities of dislocations with Burgers' vectors <110> or [001] (Figure 5). Organization of some dislocations into loose walls indicates incipient subgrain formation. Some fracture zones include crystal fragments which show surprisingly smooth boundaries that appear to have migrated short distances into surrounding high-dislocation-density matrix. Fracturing, fragmentation and subsequent migration of fragment boundaries could therefore be a way to nucleate new grains and perhaps is an unrecognised process in dynamic recrystallization.

These results agree well with observations for bulging recrystallization in quartz where, in the lowest temperature regime in nature, recrystallization is clearly associated with fracturing. There is also experimental evidence for the interaction of dislocations with fractures in quartz. Our observations in plagioclase are consistent with recent work by others, both in naturally deformed examples where new grains without host control have been recognised in fractured porphyroclasts, and in an experimentally deformed case where dislocations have interacted with fractures.

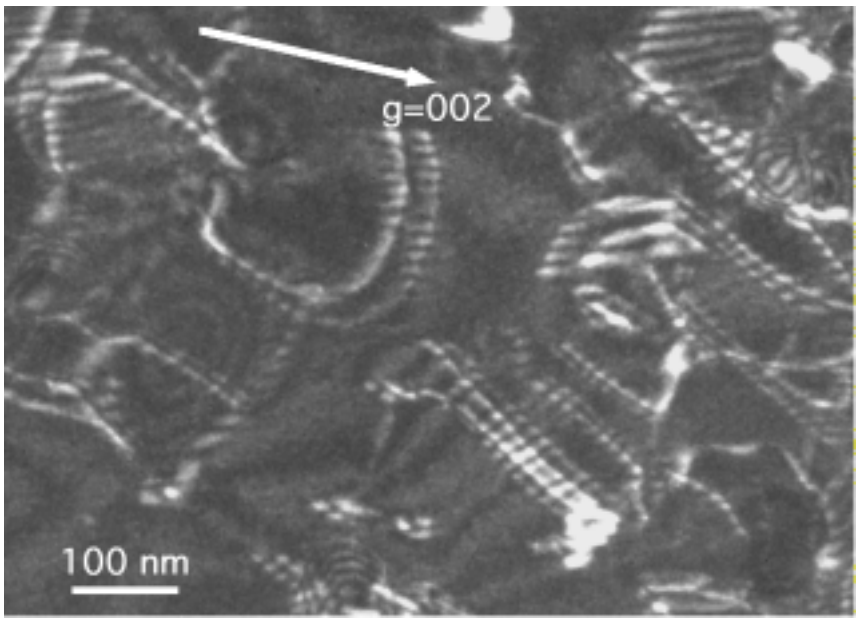

Figure 5: Micrograph from TEM showing a uniform dislocation density in a region far removed from any fractures in the experimentally deformed single crystal of plagioclase. The crystal is viewed in darkfield g=002 with the electron beam near . The dislocations having [001] Burgers' vector bend and appear to exist in pairs on the $[\bar{1}10]$ plane. They are diagnostic of the [001](010) slip system having been activated here by the applied stress.

The important points of our study are:

(1) The two most important slip systems for $C\bar{1}$ plagioclase are: [001](010) and <110> on either $(1\bar{1}\bar{1})$ or (001), similar to those seen in some earlier studies. Dislocation sources have not been identified in general.

(2) Fractures are important for the generation of some dislocations which, if glissile, can lead

to local crystal plastic deformation of the crystals. Therefore, plasticity at surprisingly low temperatures in feldspar and perhaps in other silicates could be explained by dense fracturing.

(3) Fragments from the fracture process may act as nuclei for recrystallization by grain boundary migration.

Other microstructural investigations.

The transmission electron microscope in the Petrophysics Group is operated on behalf of the ANU Electron Microscopy Unit and is an open-access facility for campus use. Consequently a wide range of materials-science projects are normally being conducted. Two examples of projects in which RSES staff have collaborated this year are listed below.

TEM Analysis of defects resulting from high-energy ion implantation

J. Wong-Leung[4], C. Jagadish[4], S. Fatima[4], J.D. Fitz Gerald, J. Zou[5] and D.J.H. Cockayne[6]

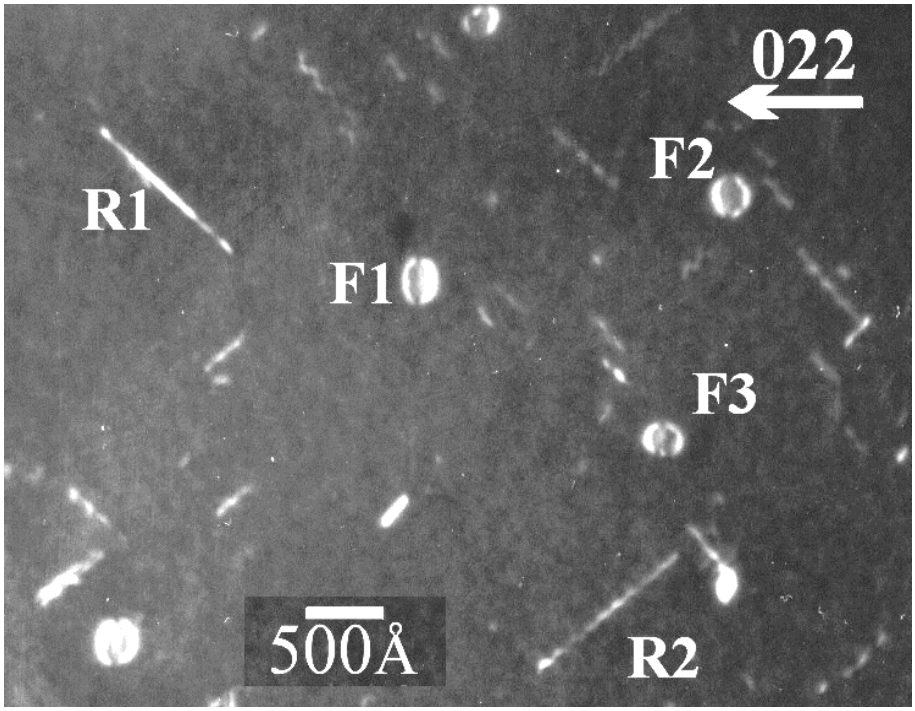

Figure 6: Micrograph from TEM of a plan-view sample of Si implanted with 1 MeV Sn to a dose of $3x10^{13}$ cm^{-2} at room temperature. Defects with R prefixes are known as rod-like defects - they lie along <110> directions and are extended on a {311} plane. Defects with F prefixes are Frank faulted loops lying on one of the {111} planes. All defects are interstitial in character.

Ion implantation is widely used commercially as a key step in microcircuit fabrication. However much remains to be established about the nature of defects produced and their generation processes. Silicon wafers have been implanted with Si, Ge or Sn ions with incident energies in the MeV range, then annealed at 800˚C for 15 mins. Defects have been characterised using both Deep Level Transient Spectroscopy and TEM. Ion doses exceeding some threshold

[4] Research School of Physical Sciences and Engineering
[5] Australian Key Centre for Microscopy and Microanalysis, University of Sydney
[6] Department of Materials, University of Oxford, England

(which is dependent on ion mass) result in extended defects that can be identified using TEM. The types and sizes of defects have been analysed by diffraction contrast analysis (Figure 6) and by crystallographic trace analysis, and their variation with depth from surface characterised. Dislocation loop defects were all found to be interstitial in nature. Trends have been identified in the proportions of different defect types as a function of ion mass and implant temperature (from –196°C to 300°C). Heavy implant species (e.g., Sn) create much denser damage cascades than do lighter species (e.g., Si). Significant dynamic annealing of implant damage occurs in the lattice of the target Si and the extent of this recovery is increased by raising the implant temperature.

Nanotubes of boron nitride

J.D. Fitz Gerald and Y. Chen[7]

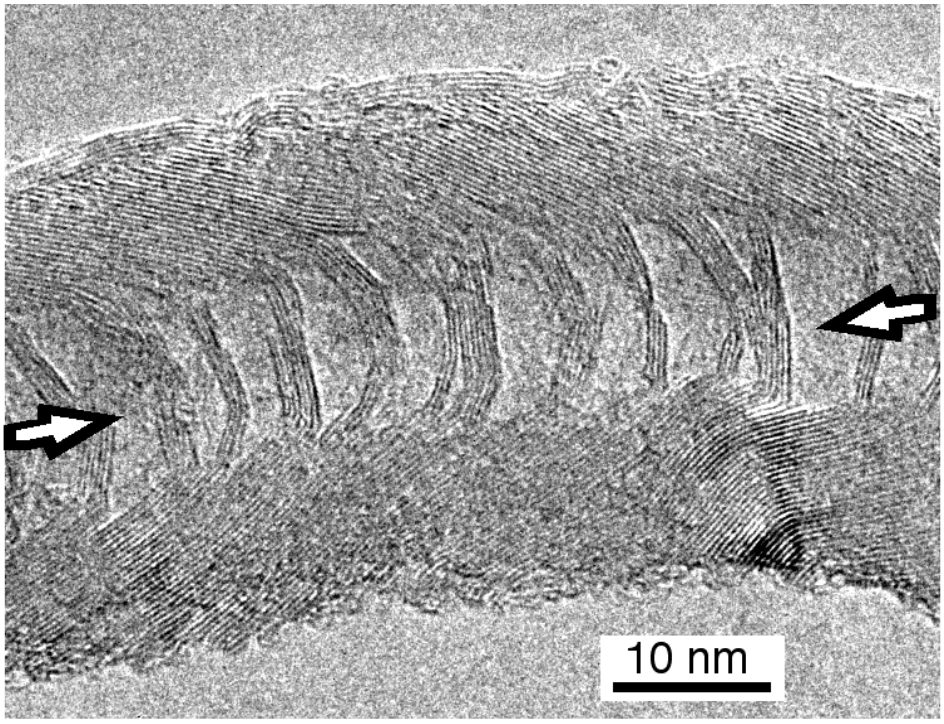

Figure 7: TEM image of one BN nanotube which has grown from a W-metal particle. The viewing direction is perpendicular to the tube axis (indicated by the two large arrows). Lattice planes ((002) of BN with interplanar spacing about 0.34 nm) curve in this image because the sheets of BN exist in three-dimensional cup-like structures and are nested one into another to make up tubes that can be micrometres in length. Layer planes are only parallel to the tube axis at the top of the image, probably due to later deposition of BN at the outer surface.

Most of the research into nanotubes, man-made tubules with diameters of a few or a few tens of nanometres, has involved their growth using carbon. However, since ordered boron nitride also crystallizes in a graphite-like structure yet has electronic properties significantly different from graphite, considerable interest has developed in nanotubes with this composition. We have previously studied boron nitride nanotubes from reactive ball milled precursors and found that Fe contamination from the stainless steel ball mill had catalysed the nanotube growth. This year, new experiments have been conducted using boron milled in a nitrogen atmosphere in a tungsten-carbide ball mill. Boron nitride nanotubes with high yield have been produced by annealing under carefully controlled furnace conditions. The microstructures of these intriguing

[7] Dept. Engineering, Faculty of Engineering and Information Technology

materials have been carefully examined with scanning and analytical transmission electron microscopy to gain insight into formation processes. Boron nitride nanotubes have been observed growing from tungsten-metal particles. This process must occur by (surface?) diffusion in the solid state since annealing temperatures are low. These tubes with diameters about 20 nm have a nested, cup-like arrangement of the boron nitride layer planes (Figure 7). We are currently experimenting with the best conditions for producing the more ideal, parallel-walled boron nitride nanotubes.

ASTEROID/COMET IMPACTS AND EARLY CRUSTAL EVOLUTION

As predicted from the cratering flux in the solar system and geological evidence, terrestrial crustal evolution has been severely perturbed by post-late heavy bombardment (post-3.8 Ga) impact by large asteroids and comets. The research reported below includes (1) a search for distal impact fallout deposits in Archaean terrains, identified by magnesian and siderophile trace element signatures in sediments and by microkrystite spherule condensates from impact-released silicate vapour (2) study of Australian multi-ring impact structures, notably the newly proven 120 km-diameter Woodleigh impact structure, and their environmental consequences, and (3) identification of the origin of circular structures under the Timor Sea.

Evidence for major 3.2 ± 0.1 Ga asteroid bombardment in the Earth-Moon system, with implications for early crustal evolution.

A.Y. Glikson, G. R. Byerly[8], D.R. Lowe[9], W. Taylor, C. Allen, I.H. Campbell

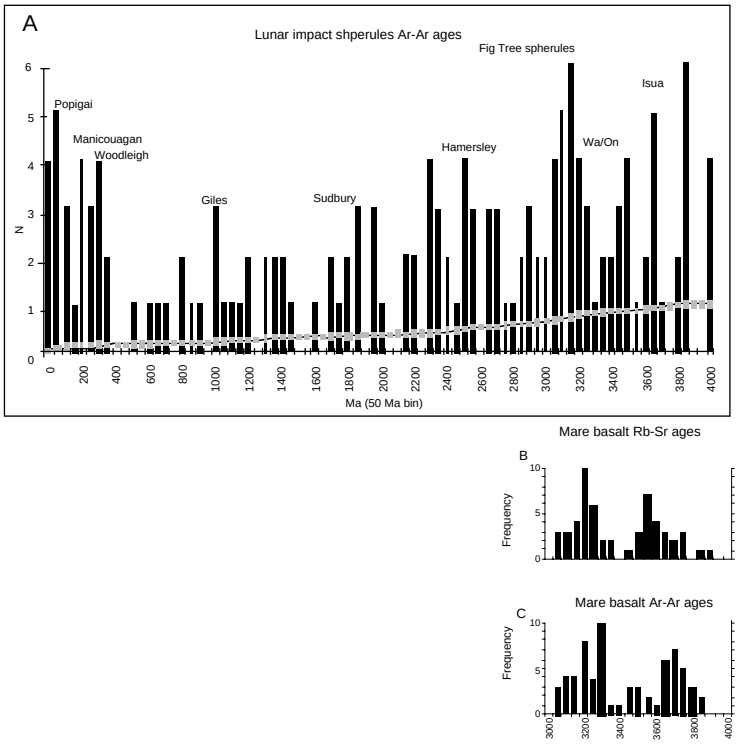

Figure 8: – (A) Frequency distribution of Ar-Ar ages of impact spherules, based on data reported by Culler et al., (2000) *Science, 287, 1785-789.* compared with frequency distribution of (B) Rb-Sr isotopic ages of mare basalts and (C) Ar-Ar isotopic ages of mare basalts (cited from Basalt Volcanism of the Terrestrial Planets). The ages of some terrestrial impact events are marked.

[8] University of Louisiana

[9] Stanford University

Evidence for up to mare-scale impact basins in the mid-Archaean from c. 3.24 - 3.225 Ga-old impact-produced vapour condensation-fallout spherule layers (microkrystites) in the Barberton greenstone belt, Transvaal is demonstrated by (1) PGE anomalies showing depletion in volatile species (Pd, Au) consistent with atmospheric condensation; (2) Ni-rich chromites (up to 23% NiO) distinct from terrestrial spinels; (3) $^{53}Cr/^{52}Cr$ ratios depleted relative to terrestrial values . Mass balance calculations based on abundance of Ir and Cr isotopes and correlations based on spherule size distribution suggest asteroid diameters in the range of 20-50 km. The chlorite-dominated spherule composition and lack of shocked quartz-bearing sial-derived fallout suggests an oceanic setting of the impacts craters scaled at 400 - 800 km diameter. This impact cluster may correspond to c. 3.18 Ga impact peak documented by laser Ar-Ar ages of lunar spherules. A peak in lunar volcanism about 3.2 Ga, suggested by Rb-Sr and Ar-Ar lunar volcanic age frequencies, may hint at a late Imbrian - Eratosthenian boundary (c. 3.2 Ga) impact-triggered basaltic volcanism within the lunar mare (Figure 8). The terrestrial and lunar data are consistent with a mid-Archaean impact cataclysm in the Earth-Moon system. An abrupt lithological change in both the Kaapvaal and Pilbara cratons from pre-3.24 Ga simatic crustal assemblages to post 3.24 Ga felsic volcanic - turbidite - granite clast-bearing conglomerates indicates a change in crustal conditions involving strong differential vertical movements expressed by rifting uplift and unroofing of granitic batholiths. Models of terrestrial crustal evolution need to take into account the inevitable magmatic and tectonic consequences of large impacts, not least where they occur in thin crustal geothermally active oceanic regimes.

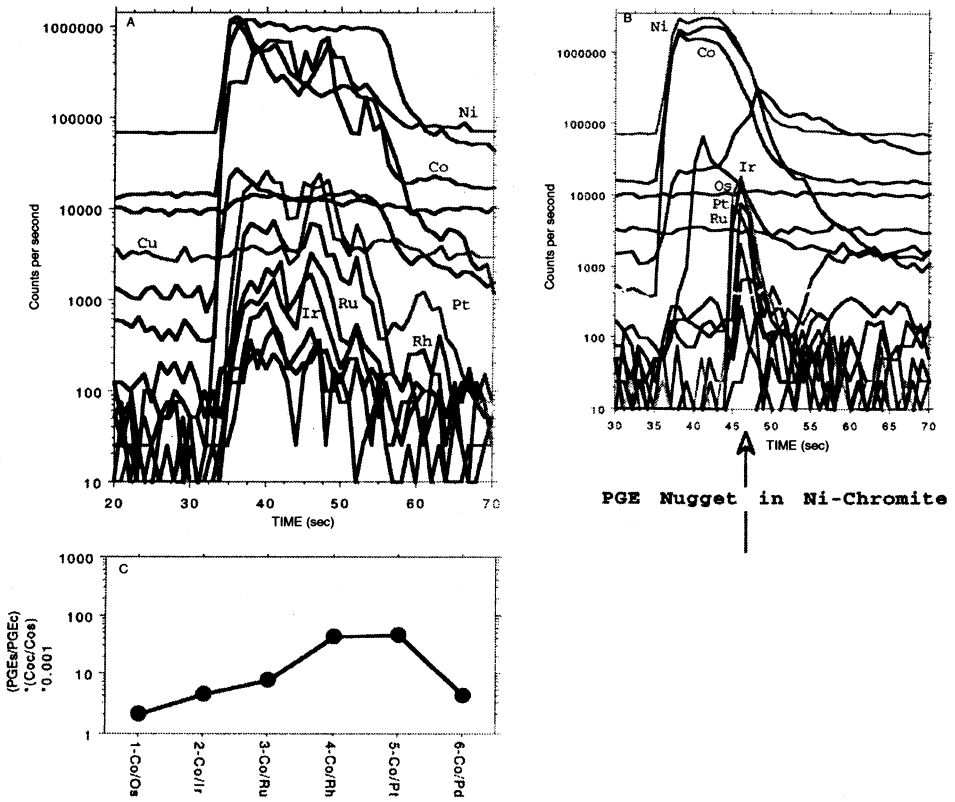

Figure 9: – Laser-ICPMS sections analyses of Ni-rich chromites from the S3 spherule unit, Barberton Mountainland, Transvaal, plotting counts per second vs time. (A) a section displaying the anomalously high Ni and Co abundance levels of a chromite grain; (C) a Cobalt-normalised and chondrite-normalised abundance profile for section A, showing relative high Pt and Rh and relatively low Pd , Ru, Ir and Os (B) a section intersecting a Platinum Group Element nano-nugget, showing extreme abundance levels of Ir, Os, Pt and Ru. Arrow on right hand diagram indicates position of PGE nugget in Ni-chromite. Analyses by W. Taylor.

Scans and laser ablation ICP-MS sections across spherules (sample SA306-1) indicate the latter are dominated by micro crystalline assemblages of Cr-rich (~0.2-0.3% Cr_2O_3) ferrous chlorite and apatite (~7-10% P_2O_5; ~8-12% CaO). Sections across Ni-chromite grains indicate substitution of Cr and Fe but little zonation of Ni and Co. Laser ablation ICP-MS sections indicate that the PGE are concentrated in nano-nuggets, showing peak Pt and Rh values (Figure 9[a]), and are depleted in Ir, Os, Ru and Pd relative to Pt and Rh (Figure 9[c]). These patterns, which differ from most terrestrial PGE patterns, probably reflect fractionation of the platinum group elements (PGE) during condensation, including loss of the volatile Pd, also reflected by depletion in Pd and Au in whole rock PGE analyses.

A search was made for equivalents of the ~3.24-3.225 Ga Barberton spherules at the base of a turbidite-felsic volcanic sequence of the c.3.24 Ga base of the Gorge Creek Group, Pilbara Block, Western Australia. The abundance of spherulitic volcanic textures, including accretionary lapilli and varioles, in felsic and mafic volcanic rocks in the Gorge Creek Group and in the c.2.78 - 2.63 Ga Fortescue Group complicates identification of impact spherules in these sequences.

Age and implications of the 120 km-diameter Woodleigh impact structure, Carnarvon Basin, Western Australia.

A.Y. Glikson, T. Uysal[10], A.J. Mory[11], R. Iasky[11], F. Pirajno[11], S.P. Kelley[12] , S. Eggins, R.A. Armstrong.

A determination of the age of the Woodleigh impact – now the world's 4th largest - was attempted using several isotopic methods. A pre-Jurassic age is indicated by overlying Early Jurassic sediments of the Woodleigh Formation, restricted to the ring synclines as well as onlapping the margins of the central uplift. The youngest deformed sediments include lower Devonian units, setting an older age limit to the impact. The isotopic systems of biotite in the basement uplift remained stable in the samples analysed, as shown by (1) a model Rb-Sr age of 835 Ma, and (2) K-Ar isotopic age of ~800 Ma, with marginal rim resetting to about 700 Ma. However, isotopic K-Ar analysis of illite and interleaved illite/smectite grains separated from granitoid of the central uplift and from basal diamictite of the inner ring syncline suggest upper Devonian ages. Thus, core sample W149148 yielded an age of 362 Ma, and K-Ar ages of illite and smectite separated from the basal diamictite at Woodleigh 2A yield late to end-Devonian ages. Infra-red laser spot fusion analysis indicates loss of potassium in pseudotachylite veins in shocked granitoid, and altered K-feldspar yielded ages mostly in the range 180-130 Ma, reflecting post-impact burial. The diamictite contains shale clasts containing early Permian palynomorphs, probably representing sedimentary mixing in the ring syncline. It follows that the Woodleigh impact structure is of late to end-Devonian age.

Woodleigh thus constitutes the largest member of a late Devonian impact cluster, which also includes Charlevoix (Quebec), Siljan (Sweden), Ternovka (Ukraine), Kaluga (Russia), Ilynets (Ukraine), and Elbow (Saskatchewan). Iridium anomalies related to the late Devonian (Frasnian-Fammenian boundary) events are known from the north Canning Basin, Western Australia, microtektites are found along this boundary in south China, and marked 13/12C excursions occur in Alberta. This extinction saw the elimination of rugose coral reefs, trilobites, ammonoids, brachiopods and conodont species, including destruction of the Devonian reefs which fringe the Kimberley Block, north Western Australia. A search is planned for tsunami deposits along the late Devonian boundary in the Gascoyne Province.

Laser ablation ICP-MS and electron microscopy and microprobe studies of pseudotachylite and impact melt-injected shock-metamorphosed granitoid from the uplifted basement core of Woodleigh confirm earlier indications of anomalous siderophile and magnesian element abundances (Mg, Fe, Ni, Cr, Co, V) in the pseudotachylite and diaplectic

[10] University of Queensland
[11] Geological Survey of Western Australia
[12] Open University, Milton Keynes, U.K.

glass inclusions within feldspar. In the absence of ultramafic rocks in the vicinity, it is suggested the anomalous ultramafic chemistry is related to injection of melt and condensation of vapour phases derived from the exploding projectile.

A post-Eocene pre-Miocene lamproite diatreme field, Timor Sea, Northern Australia

A.Y. Glikson, J.D. Gorter[13], W. Taylor

An earlier report on a probable impact connection of the Fohn structure, Timor Sea was based on (1) identification of a 4.8 km-diameter craterform cored by a central uplift by 1-km grid seismic reflection data; (2) siderophile element anomalies (Ni < 428 ppm; Co < 51 ppm; Cr < 518) in drill chips from Fohn-1 well located east of the central core, and (3) presence of Cretaceous foraminifera in the cuttings, which suggested deep crater excavation. Further petrological studies of Fohn drill cuttings from depths of 850-860 m and 870-880 m uncovered apatite-rich leucite-olivine lamproite assemblages consisting of pseudomorphs of analcite after leucite, talc/chlorite-altered olivine, diopside, Ti-phlogopite, Sr-apatite, Mg-ilmenite, priderite, rutile, and secondary barite. These observations, consistent with high gamma anomalies, shed new light on the origin of the Fohn structure and an associated field of over 40 crater-form and bulge-form circular structures along the post-Eocene pre-Miocene unconformity under the Timor Sea. Earlier interpretation in terms of impact origin resulted from remarkable analogies between Fohn structure and impact structures, including (1) similarity between the centrally cored annular syncline seismic structure of lamproite diatremes and central uplifts of impact structures; (2) similarities between altered siderophile element-enriched chemistry of drill cuttings and meteoritic contamination; (3) transport of Cretaceous foraminifera from deep-diatreme levels interpreted earlier in terms of deep impact crater excavation.

The Fohn lamproites can be classified in terms of parameters defined in Mitchell and Bergman. On the basis of Mg# (Mg/Mg+Fe) (~57-69%), SiO_2 (~44-52%) and K_2O (~5-8%) the rocks correspond to the field of phlogopite leucite melanophonolites similar to the field of West Kimberley lamproites (Mg# ~ 50-75; SiO_2 ~ 45-58%). Many Fohn rocks also have moderate CaO levels of ~ 4-5% similar to the West Kimberley, although some Fohn analyses show higher CaO levels (7-13% CaO), mostly reflecting their high apatite abundances (P_2O_5 1-6%). In this respect the Fohn lamproites are distinct from West Kimberley lamproites, with P_2O_5 levels rarely above ~2.0%. Fohn lamproites are also high in FeO (~8-10%) and TiO_2 (~5-12%) levels of some of these rocks, reflecting their high ilmenite, priderite and rutile contents.

[13] British-Borneo Australia Limited